THE ASTROPHYSICAL JOURNAL, 483:947–960, 1997 July 10

THE X-RAY SUN IN TIME: A STUDY OF THE LONG-TERM EVOLUTION OF CORONAE OF SOLAR-TYPE STARS

MANUEL GÜDEL
Paul Scherrer Institut, Würenlingen und Villigen, CH-5232 Villigen PSI, Switzerland; guedel@astro.phys.ethz.ch

EDWARD F. GUINAN
Department of Astronomy and Astrophysics, Villanova University, Villanova, PA 19085; guinan@ucis.vill.edu

AND

STEPHEN L. SKINNER[1]
ISAS, 3-1-1 Yoshinodai, Sagamihara, Kanagawa 229, Japan; skinner@jila.colorado.edu
Received 1996 August 26; accepted 1997 February 6

ABSTRACT

We have used the *ASCA* and *ROSAT* X-ray satellites to probe the coronae of a sample of nine solar-like G stars. These stars are all ostensibly single with ages ranging from 70 Myr to 9 Gyr and have X-ray luminosities ranging from 1 to 500 times that of the quiet Sun. Specifically, we investigate the dependence of the coronal temperature and emission measure structure of these stars on age and rotation period.

In the younger stars, a considerable portion of the volume emission measure resides at very high temperatures, reaching up to ∼20–30 MK in EK Dra. Such temperatures are comparable to temperatures that are achieved on the Sun during short flaring episodes. In two-temperature fits to *ROSAT* data, the higher temperature decays rapidly within the first few 100 Myr; the decay may be described by an inverse power law, $T_{\rm hot} \propto {\rm age}^{-0.3}$. We also find a power-law dependence between the total X-ray luminosity and the higher temperature $L_{\rm X} \propto T_{\rm hot}^4$. We interpret this as evidence of a decrease in the efficiency of high-temperature coronal heating as a solar-like star ages and its rotation slows down. A reconstruction of the coronal differential emission measure (DEM) distribution in three of the stars using *ASCA* data indicates a bimodal distribution in temperature, with the hotter plasma at 12–30 MK and the cooler plasma below 10 MK. We infer, for the first time, a consistent evolution of the DEM structure in a solar-type star. The emission measure of the hotter component rapidly decreases with age and becomes unimportant at ages beyond ∼500 Myr. The emitted X-ray emission of the young Sun thus rapidly softened, which had important implications for the young planetary atmospheres. We suggest that the high-temperature component is the result of superimposed but temporally unresolved flaring events and support this picture by reconstructing the time-integrated (average) emission measure distribution of a typical solar X-ray flare. Radio observations of active stars fit well into this picture and suggest that the presence of nonthermal electrons in coronae is linked to the presence of hot (>10 MK) plasma, very much the same situation as in solar flares. We find, however, that radio emission saturates, if at all, at smaller rotation periods than does X-ray emission.

Subject headings: stars: coronae — stars: evolution — Sun: corona — Sun: flares — X-rays: stars

1. INTRODUCTION

The Sun's magnetic activity and consequently its chromospheric and coronal emissions are expected to have declined steadily to present levels as the solar rotation slowed owing to magnetic braking (Skumanich 1972; Simon, Herbig, & Boesgaard 1985). Despite the fact that evolutionary models indicate that the zero-age main-sequence (ZAMS) Sun had a bolometric luminosity smaller than the present Sun ($L_{\rm ZAMS} \approx 0.76\ L_\odot$), young solar-type stars maintain X-ray luminosities up to at least 2 orders of magnitude higher than the nonflaring Sun (see, e.g., Micela et al. 1985; Caillault & Helfand 1985; Maggio et al. 1987; Schmitt et al. 1990; Dorren & Guinan 1994a; Dorren, Güdel, & Guinan 1995). The increased level of magnetic activity is also reflected in more frequent strong flaring and in enhanced levels of optical/UV emission lines and nonthermal radio emission. An extensive account of the current knowledge about various aspects of the "Sun in Time" has been given in Sonett, Giampapa, & Matthews (1991). The role of declining magnetic activity during the spin-down of a main-sequence star is summarized in, among others, Walter & Barry (1991) or Simon (1992).

We have initiated a comprehensive project on "The Sun in Time" (Dorren & Guinan 1994a), devoted to the study of the long-term evolution of the observable physical properties (e.g., temperature, emission measure distribution, and magnetic fields) of the outer atmosphere of a main-sequence early G star between the zero-age main sequence (ZAMS) and the terminal-age main sequence (TAMS). The importance of fundamental stellar properties (such as convection zone depth, stellar rotation, chemical composition, or surface gravity) for X-ray emission characteristics is well known from a phenomenological point of view (Pallavicini et al. 1981; Walter 1981; Schmitt et al. 1985, 1990; Simon & Landsman 1991; Barbera et al. 1993; and others). By selecting a star sample narrowly confined in spectral type, we can infer the long-term evolution of the solar atmosphere with a minimum of systematic effects from such variable properties.

The observable soft X-ray emission of stellar coronae provides a number of important diagnostics to characterize

[1] Present address: JILA, University of Colorado, Boulder, CO 80309-0440.

physical mechanisms responsible for coronal heating. Previous studies have indicated that coronae of magnetically highly active stars tend to be hotter than coronae of low-activity analogs (see, e.g., Schrijver, Mewe, & Walter 1984; Schmitt et al. 1990; Schmitt, Fleming, & Giampapa 1995; Jordan & Montesinos 1991; Gagné, Caillault, & Stauffer 1995). The cause for this correlation has not been studied in detail; for most stars, data from previous X-ray detectors (on board *ROSAT* and *Einstein*) were not optimized to determine unambiguously to what extent these temperatures are physical temperatures of isothermal plasmas or whether the measurements rather represent a weighted average of a more complex emission measure distribution.

More recently, results from observations of active stars with the medium-resolution *EUVE* and *ASCA* satellites, but also the transmission grating spectrometer on board *EXOSAT*, have provided evidence that the coronal plasma can be distributed over a considerable range of temperatures. Differential emission measure (DEM) distributions with one global maximum or two maxima separated by a deep local minimum have been reported most frequently for a number of stellar types at different activity levels (see, e.g., Lemen et al. 1989; Dupree et al. 1993; Schrijver et al. 1995; Rucinski et al. 1995; Drake, Laming, & Widing 1995; Dupree, Brickhouse, & Hanson 1996; Brickhouse 1996; Mewe et al. 1996, 1997; Kaastra et al. 1996a); clearly, results from simplified approaches, like isothermal or 2-T (two-temperature) fits to low-resolution spectral data, should be interpreted with caution (see the comparative study by Schmitt et al. 1990). The example of the nonflaring Sun illustrates also quite clearly that its coronal DEM covers a considerable range of temperatures (see, e.g., Raymond & Doyle 1981; Bruner & McWhirther 1988).

The temperature structuring of coronae of solar-type stars is potentially important to link solar concepts to stars like the Sun but at different activity levels. For example, the possible role of flares in coronal heating to very hot temperatures (>10 MK) has been discussed ever since the unambiguous detection of such hot material in the apparently quiescent phases of active stars, and its concurrence with other flarelike phenomena (see, e.g., Lemen et al. 1989; Güdel 1994; Schrijver et al. 1995; Giampapa et al. 1996). In the most rapidly rotating magnetically active stars, a phenomenon commonly referred to as "saturation" occurs; the chromospheric and coronal emissions reach a maximum that cannot be exceeded even if the star would spin up further. Saturation of hot coronae may be a signature of a stellar surface that is completely covered with active region coronal loops with appreciable densities (see, e.g., Vilhu 1984; Vilhu & Walter 1987).

The present paper gives a comprehensive account on the X-ray view of our project based on *ROSAT* and *ASCA* observations. Previous reports on the overall project including optical photometry and spectroscopy as well as UV observations can be found in Dorren & Guinan (1994a, 1994b); the radio domain has been discussed by Güdel, Schmitt, & Benz (1994, 1995a) and Güdel et al. (1995b). Reports on particular X-ray aspects can be found in Dorren et al. (1995; a ZAMS and a TAMS Sun in X-rays), Güdel & Guinan (1996), and Güdel, Guinan, & Skinner (1996b; aspects of results from *ROSAT*).

2. TARGETS

The present study has evolved from a carefully selected sample of near-solar–type main-sequence stars; Dorren & Guinan (1994a) defined the program stars together with principal aims of the project. The latter include (1) investigating the evolution of the solar dynamo and solar magnetic activity from the ZAMS to the TAMS age; (2) establishing the extent to which the Sun is typical of stars of its age and spectral type; and (3) obtaining estimates of the solar UV and X-ray emission fluxes throughout the Sun's post-ZAMS history. We list the properties of all program stars in Table 1, including the indicators from which approximate ages were derived. The stars were selected mainly for their well-established rotation periods (as chiefly measured by optical photometry; Dorren & Guinan 1994a; Guinan et al. 1997 in particular for α Cen A and β Hyi) and reliably determined ages (partly supported by cluster or moving group memberships, age-rotation relations, and isochronal ages).

The principal free parameter in our star sample is the rotation period $P_{\rm rot}$ (or the age), with all other fundamental properties being as close to solar as possible (e.g., mass and radius and therefore surface gravity, chemical composition, convection zone depth except for some evolutionary effects). The oldest star of the sample, β Hyi, is classified as a subgiant at a position in the H-R diagram that represents the Sun when it will be leaving the main-sequence branch

TABLE 1
PROGRAM STARS

Star	HD	HR	Spectral Type	Distance (pc)	$P_{\rm rot}$ (d)	Age (Gyr)	Age, Indicator, Membership
EK Dra	129333	...	G0 V	31	2.75	0.07	Pleiades moving group
π^1 UMa	72905	3391	G1.5 V	14	4.68	0.3	Ursa Major stream
HN Peg	206860	8314	G0 V	15.1	4.86	0.3	Rotation-age relationship[a]
χ^1 Ori	39587	2047	G1 V	10.0	5.08	0.3	Ursa Major stream
BE Cet	1835	88	G2 V	20.4	7.65	0.6	Hyades moving group
VB 64	28099	...	G2 V	46.6	8.7	0.6	Hyades cluster member
κ^1 Cet	20630	996	G5 V	9.3	9.2	0.75	Rotation-age relationship[b]
β Com	114710	4983	G0 V	8.1	12.4	1.6	Rotation-age relationship
15 Sge	190406	7672	G5 V	17.2	13.5	1.9	Rotation-age relationship
Sun	...	...	G2 V	1 AU	25.4	4.6	Isotopic dating on Earth
α Cen A	128620	5459	G2 V	1.33	~30	5–6	Isochrones, rotation
β Hyi	2151	98	G2 IV	6.5	~28[c]	9	Isochrones[d]

[a] Same rotation period as UMa stream G0 V members.
[b] Possible member of the Hyades moving group.
[c] New period determined by Guinan et al. 1997.
[d] Isochrone age from Dravins et al. 1993c.

(Dravins et al. 1993c). Its properties differ somewhat from typical younger main-sequence G-star properties; e.g., it has expanded to a radius of 1.6 $R_\odot$, and it shows subsolar photospheric metal abundances (Dravins et al. 1993c).

We list, without intending to be complete, exemplary studies or surveys that contain some previous X-ray observations of our targets: Maggio et al. (1987; *Einstein* luminosities of most of our targets); Schmitt et al. (1990; *Einstein* luminosities and temperatures from 2-T fits); Ayres et al. (1995; *ROSAT* X-ray All-Sky Survey [RASS] fluxes of a few targets); Schmitt (1997; X-ray fluxes and hardness ratios from the RASS for a few targets); Landini et al. (1986; *EXOSAT* study of π^1 UMa), Dravins et al. (1993a, 1993b, 1993c, detailed study of β Hyi including *EXOSAT* results); and Dorren et al. (1995; detailed pointed *ROSAT* PSPC investigation of EK Dra and β Hyi). To extend our investigation to the most rapidly rotating solar-type stars, we will complement our data set with published results of rapidly rotating, very young main-sequence stars or of pairs of synchronously rotating solar-type stars in close orbits.

3. OBSERVATIONS

For seven of the program stars, we have obtained pointed *ROSAT* PSPC observations as part of the *ROSAT* Guest Observer program. A log of observations is presented in Table 2. Two targets (EK Dra and β Hyi) were observed repeatedly in order to search for long-term variations in the X-ray output that may be due to magnetic activity cycles (Dorren et al. 1995). The observation of χ^1 Ori was retrieved from the *ROSAT* archive (project ID 200794); this is the only observation presented here that made use of the boron filter in front of the PSPC to suppress the softer emission. A description of the *ROSAT* PSPC instrument can be found in Pfefferman et al. (1986). Specifically, *ROSAT* observes between 0.1 and 2.4 keV with an energy resolution of approximately $E/\Delta E = 2$. Its effective area peaks around 0.3 keV and around 1 keV, reaching approximately 250 cm^2.

For the younger stars EK Dra (age $\approx$ 70 Myr), HN Peg ($\sim$300 Myr), and κ^1 Cet ($\sim$750 Myr), we obtained *ASCA* observations in the *ASCA* Guest Observer program. A description of the *ASCA* mission and its detectors can be found in Tanaka, Inoue, & Holt (1994). *ASCA* carries four identical X-ray telescopes (XRTs) that feed two Solid-State Imaging Spectrometers (SIS0 and SIS1) and two Gas Imaging Spectrometers (GIS2 and GIS3). The SIS detectors are sensitive to 0.4–10 keV photons with an effective area (combined with XRT) of up to 200 cm^2 per SIS at 1.5 keV. The SIS energy resolution is approximately 3% (FWHM) at 6.7 keV, scaling roughly as (energy)$^{-1/2}$. The GIS detectors are sensitive to higher energies, comprising the $\sim$0.6–12 keV range with a maximum effective area of $\sim$170 cm^2 at about 2 keV.

4. DATA ANALYSIS AND RESULTS

4.1. *Data Analysis*

All *ROSAT* data were reduced in the MIDAS/EXSAS analysis software package using standard procedures. Spectral fits were performed in the XSPEC software package, using the Raymond-Smith (RS) code (Raymond & Smith 1977; Raymond 1988) and the Mewe-Kaastra-Liedahl (MEKAL) code (Mewe, Gronenschild, & van den Oord 1985; Mewe, Kaastra, & Liedahl 1995). If necessary, interstellar hydrogen absorption columns were included in the models as free fitting parameters. Average backgrounds were subtracted from the spectra. The *ASCA* data presented here were reduced in the FTOOLS/XSELECT package and fitted in XSPEC (multitemperature fits applying the MEKAL models). Our fit results were derived from simultaneous fits to both SIS spectra. In the case of HN Peg, the star's position on the SIS1 chip 3 was relatively close to the interchip gap. We therefore did not combine the two SIS data sets and mostly relied on the safer SIS0 results. The unprecedented spectral resolution *and* sensitivity of the *ASCA* SIS spectrometers in principle allow us to derive emission measures (EMs) of a series of plasma components over a wide range of temperatures ($\sim$2–100 MK) and, if no standardized elemental abundance table is used, to estimate coronal abundances through fits to line blends and the overall spectral shape. The limited number of independent spectral "channels" generally implies a trade-off between the number of plasma components and the number of freely adjustable elemental abundance parameters. In our case, the number of fitted elemental abundances was itself restricted since the available signal-to-noise ratio did not permit to derive abundances of elements like Ca, Ar, Al, N, C, and others unambiguously. Preference was given to ele-

TABLE 2

OBSERVING LOG

Target	Satellite	Date (yy/mm/dd)	Exposure Time[a] (s)	Count Rate[b] (counts s^{-1})
EK Dra[cd]	*ROSAT*	93/10/19	5157	0.864 ± 0.013
	ASCA	94/05/24	14830	0.180 ± 0.0035
π^1 UMa	*ROSAT*	93/10/05	4988	0.879 ± 0.014
HN Peg	*ASCA*	95/10/05	11872	0.077 ± 0.0027
χ^1 Ori	*ROSAT*	92/05/04	5274	0.408 ± 0.009[e]
BE Cet	*ROSAT*	93/06/16	5488	0.404 ± 0.009
κ^1 Cet	*ROSAT*	93/07/27	1676	1.076 ± 0.0026
	ASCA	94/08/16	17780	0.098 ± 0.0023
β Com	*ROSAT*	93/06/17	8374	0.358 ± 0.0069
15 Sge	*ROSAT*	93/11/14	5926	0.065 ± 0.0037
β Hyi[c]	*ROSAT*	91/05/11	1906	0.105 ± 0.0079

[a] Only useful exposure time quoted; for *ASCA*, average for SIS0 and SIS1 (for HN Peg: only SIS0).
[b] Background subtracted. For *ASCA* EK Dra and κ^1 Cet, average of SIS0 and SIS1; for *ASCA* HN Peg, SIS0 only.
[c] For previous observations, see Dorren et al. 1995.
[d] See also Güdel et al. 1997.
[e] With PSPC boron filter.

ments with distinct features in the well-observed energy range (Fe around 1 keV, Mg at $\sim$1.4 keV, Si at $\sim$1.8 keV, and S at $\sim$2.4 keV), but other elements were investigated as well.

Recalling the complex and somewhat uncertain present situation with regard to solar and stellar coronal abundances (see reviews by White 1996 and Drake 1996), we adopted a conservative strategy by starting with solar photospheric abundances and allowing elemental deviations only after fitting a number of temperatures and EMs to the *ASCA* SIS spectra. For the *ROSAT* observations, we kept with the tradition of using solar photospheric values owing to the lack of any unambiguous features on which elemental abundances can be calibrated (but see the exception of β Hyi below). Given that Fe is the most dominant metal in the X-ray regime and *ASCA* indicates that a solar photospheric value for Fe leads to excellent fits, we believe that this approach is well justified and the least ambiguous one.

We also performed a differential emission measure (DEM) analysis of the *ASCA* data with the public version of the newly developed SPEX software (Version 1.10; Kaastra, Mewe, & Nieuwenhuijzen 1996b). We used a temperature grid from approximately 10^6 to 10^8 K for the combined SIS data. We define the DEM as $D(T) = n_e n_H dV/d(\log T)$ (n_e, and n_H are the electron and hydrogen densities, respectively, and V is the emitting volume). Although we will use the DEM designation, our illustrations will display the emission measure integrated over the bin width, i.e., $\Delta(\mathrm{EM}) = D(T)\Delta \log T$ (with $\Delta \log T = 0.1$ in our examples).

A number of different approaches to reconstruct the DEM distribution were applied to the EK Dra *ASCA* and *EUVE* data by Güdel et al. (1997), with the result that all methods converge to basically the same result. Here, we confine ourselves to the presentation of the *ASCA* results from the polynomial DEM reconstruction as incorporated in SPEX. Analogous DEM reconstructions using the same spectral code have been performed for a number of X-ray–emitting stars, and for further reading, we refer the reader to Mewe et al. (1996, 1997) and Kaastra et al. (1996a).

4.2. *Results from ROSAT Observations*

In Figure 1, an age sequence of *ROSAT* spectra of the observed G stars is shown, with each spectrum renormalized to a constant flux amplitude of the lower energy peak. The nonflaring solar corona was modeled using the continuous emission measure distribution given in Raymond & Doyle (1981) between 1 and 5 MK; the modeled solar spectrum was folded with the *ROSAT* PSPC response matrix, and noise was added so as to simulate a realistic stellar observation. All spectra were fitted with two RS-type thermal plasma components; the fits are shown as histograms in Figure 1. Note that β Hyi's X-ray luminosity L_X is close to the Sun's, despite the former's significantly higher age (9 Gyr; Dravins et al. 1993c; see Table 3). But we note that β Hyi has, as a consequence of its leaving the main sequence, expanded to a radius of 1.6 $R_\odot$. Its surface X-ray flux density is, however, only 40% that of the Sun's. Assuming that the surface flux density is the critical variable of coronal activity, we renormalized β Hyi's L_X to one solar radius. Also, we adopted its subsolar photospheric metal abundance for the coronal plasma, i.e., $[\mathrm{Z/H}] = -0.2$ (Dravins et al. 1993c).

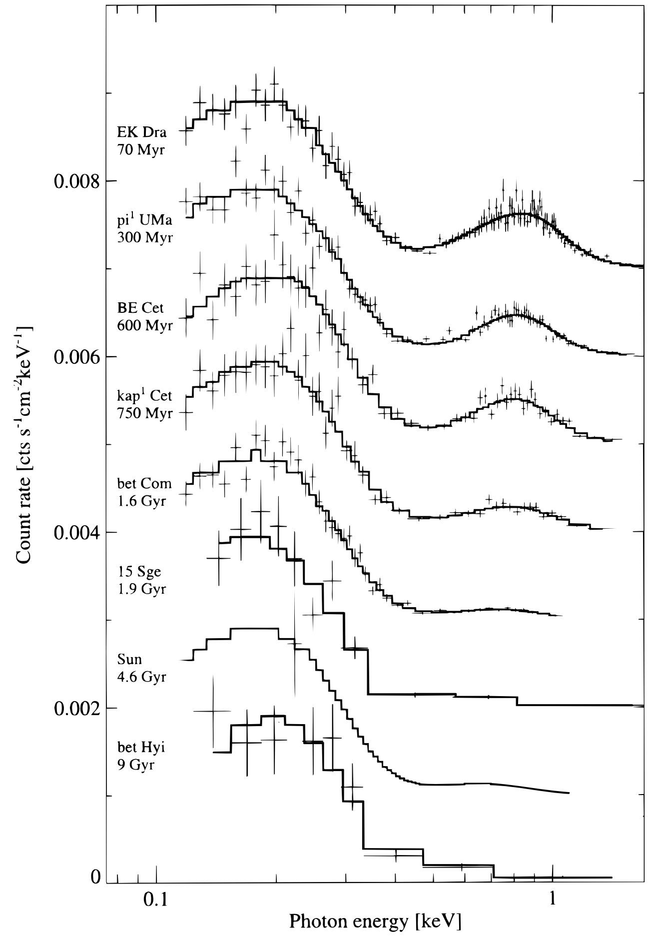

FIG. 1.—*ROSAT* PSPC pulse-height spectra of the solar proxy age series, normalized such that the amplitude of the left (lower energy) peak is equal for all spectra. Individual spectra have been shifted by multiples of 0.001 counts $\mathrm{s^{-1}\ cm^{-2}\ keV^{-1}}$ for illustration. Age monotonically increases from top (EK Dra: 70 Myr) to bottom (β Hyi: 9 Gyr). The consistent decrease of hard emission in the peak around 0.8 keV indicates a decrease in EM at high T. Crosses are observations, while histograms represent fit (2-T RS; see Table 3).

In our stars, the low-energy spectral peaks contain photons from both plasma components, while the bump around 0.8 keV is largely determined by hot (5–30 MK) plasma. Quite evidently, the relative amount of hot plasma and therefore hard radiation diminishes with age or increasing rotation period.

Figure 2 shows the numerical fit results (using the RS code). The higher temperature decreases from around 10 MK for rapidly rotating stars ($P_{\mathrm{rot}} \approx 2$ days) to $\sim 2-3$ MK for slow rotators. For T_{hot}, we thus find a decay law (based on RS or MEKAL fits)

$$T_{\mathrm{hot}} = 19.0 P_{\mathrm{rot}}^{-0.60 \pm 0.06} [\mathrm{MK}] \quad (\mathrm{RS}) \tag{1}$$

$$T_{\mathrm{hot}} = 13.6 P_{\mathrm{rot}}^{-0.50 \pm 0.05} [\mathrm{MK}] \quad (\mathrm{MEKAL}) , \tag{2}$$

where P_{rot} is in days and T_{hot} is in MK. The number of points used on the P_{rot}-T_{hot} plane is $N = 9$, and the correlation coefficient is $R = -0.929$ and $R = -0.947$ for RS and MEKAL, respectively. On using a rotation-age relation for G stars, $\log t = 1.75 \log P_{\mathrm{rot}} - 1.81$ (t in Gyr, P_{rot} in days; Dorren, Guinan, & DeWarf 1997), we find

$$T_{\mathrm{hot}} = 4.55 t^{-0.34} [\mathrm{MK}] \quad (\mathrm{RS}) \tag{3}$$

$$T_{\mathrm{hot}} = 4.10 t^{-0.29} [\mathrm{MK}] \quad (\mathrm{MEKAL}) . \tag{4}$$

TABLE 3

ROSAT 2-T Fit Results (RS and MEKAL)[a]

Star	log L_X [b] (ergs s^{-1})	T_1 (MK)	T_2 (MK)	log EM_1 (cm^{-3})	log EM_2 (cm^{-3})	EM_2/EM_1	χ^2/dof
EK Dra	29.87	$2.29^{+0.34}_{-0.29}$	$9.33^{+0.67}_{-0.78}$	$52.04^{+0.05}_{-0.06}$	$52.11^{+0.04}_{-0.05}$	$1.16^{+0.32}_{-0.23}$	93/86
	29.83	$2.24^{+0.40}_{-0.37}$	$7.68^{+1.14}_{-0.78}$	$51.92^{+0.14}_{-0.13}$	$52.15^{+0.04}_{-0.05}$	$1.74^{+0.77}_{-0.64}$	96/86
π^1 UMa	29.09	$1.41^{+0.14}_{-0.12}$	$6.35^{+0.71}_{-0.71}$	$51.24^{+0.05}_{-0.07}$	$51.30^{+0.05}_{-0.03}$	$1.15^{+0.36}_{-0.20}$	88/71
	29.07	$1.25^{+0.19}_{-0.24}$	$5.56^{+0.61}_{-0.54}$	$51.16^{+0.03}_{-0.04}$	$51.45^{+0.03}_{-0.03}$	$1.97^{+0.32}_{-0.27}$	87/71
HN Peg	28.95	...	...	...	...	...	...
χ^1 Ori	29.14	$1.43^{+0.18}_{-0.23}$	$7.49^{+0.54}_{-0.53}$	$51.43^{+0.06}_{-0.09}$	$51.25^{+0.02}_{-0.03}$	$0.65^{+0.20}_{-0.11}$	71/56
	29.08	$1.21^{+0.29}_{-0.55}$	$6.36^{+0.63}_{-0.62}$	$51.32^{+0.09}_{-0.12}$	$51.37^{+0.03}_{-0.03}$	$1.13^{+0.45}_{-0.28}$	69/56
BE Cet	29.13	$1.62^{+0.26}_{-0.37}$	$6.52^{+0.98}_{-01.2}$	$51.37^{+0.08}_{-0.11}$	$51.27^{+\cdots}_{-0.05}$	$0.79^{+\cdots}_{-0.20}$	55/47
	29.12	$1.47^{+0.50}_{-0.88}$	$5.49^{+1.12}_{-1.15}$	$51.28^{+\cdots}_{-0.17}$	$51.44^{+0.13}_{-0.08}$	$1.45^{+1.43}_{-\cdots}$	57/47
VB 64	28.90	...	...	...	...	...	...
κ^1 Cet	28.82	$1.74^{+0.20}_{-0.25}$	$7.21^{+1.6}_{-1.9}$	$51.17^{+0.06}_{-0.08}$	$50.82^{+0.06}_{-0.07}$	$0.44^{+0.18}_{-0.11}$	32/38
	28.78	$1.66^{+0.30}_{-0.41}$	$5.63^{+1.8}_{-1.6}$	$51.06^{+0.09}_{-0.11}$	$51.00^{+0.15}_{-0.11}$	$0.88^{+0.70}_{-0.33}$	31/38
β Com	28.11	$1.24^{+0.11}_{-0.11}$	$3.66^{+1.6}_{-0.57}$	$50.52^{+0.08}_{-0.05}$	$50.17^{+0.12}_{-0.22}$	$0.45^{+0.21}_{-0.23}$	34/37
	28.09	$1.15^{+0.18}_{-0.14}$	$3.48^{+1.1}_{-0.47}$	$50.53^{+0.05}_{-0.04}$	$50.29^{+0.09}_{-0.16}$	$0.56^{+0.22}_{-0.21}$	33/37
15 Sge	28.05	$1.06^{+0.38}_{-0.36}$	$3.68^{+1.9}_{-2.0}$	$50.41^{+0.14}_{-\cdots}$	$50.19^{+0.36}_{-0.41}$	$0.60^{+\cdots}_{-0.43}$	7.4/7
	28.03	$0.93^{+\cdots}_{-0.29}$	$3.47^{+3.3}_{-0.93}$	$50.49^{+0.11}_{-0.14}$	$50.27^{+0.21}_{-0.33}$	$0.60^{+0.75}_{-0.38}$	7.4/7
Sun[c]	27.3	$1.22^{+0.15}_{-0.11}$	$3.03^{+0.56}_{-0.32}$	49.63	49.50	0.74	...
α Cen A	27.11	...	...	...	...	...	...
β Hyi	27.08[d]	$2.09^{+0.31}_{-0.18}$	...	$50.20^{+0.06}_{-0.06}$	...	...	7.3/8
	27.04[d]	$2.20^{+0.21}_{-0.23}$	...	$50.19^{+0.06}_{-0.08}$	...	...	7.6/8

[a] First and second line for each star refer to RS and MEKAL fits, respectively.

[b] L_X values refer to the 0.1–2.4 keV energy range and are from the present observations, or Güdel et al. 1995a (HN Peg), or Hempelmann et al. 1995 (VB 64), or Dorren & Guinan 1994a (α Cen A).

[c] Solar data adapted from Raymond & Doyle 1981. $T_{1,2}$ are fits to an approximate model of the nonflaring solar corona; $EM_{1,2}$ are adjusted such that log $L_X = 27.3$.

[d] L_X for β Hyi scaled to one solar radius.

The nearly consistent decrease of the EM ratios for the hotter stars (i.e., EM_{hot}/EM_{cool}; squares in Fig. 2) further suggests that the hotter plasma becomes less abundant and thus that the distribution of plasma falls off increasingly steeper with age (starting from nearly flat in young stars). We will find more evidence for this in our *ASCA* data. We

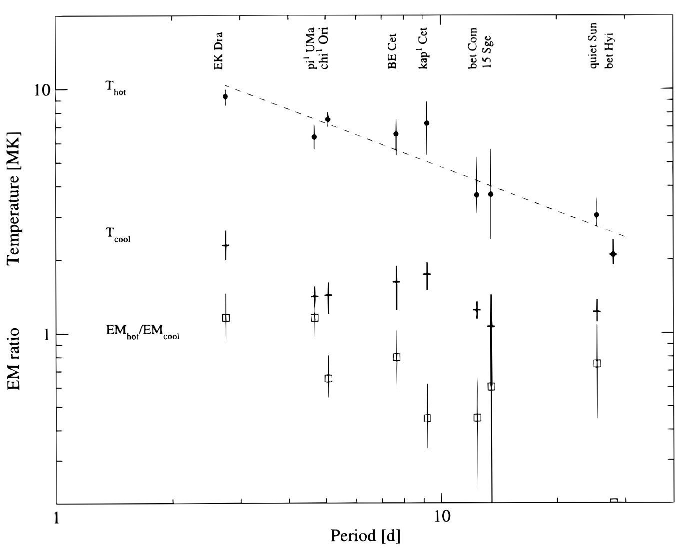

Fig. 2.—Coronal temperatures $T_{hot,cool}$ and ratios of EM for the program stars, plotted vs. their rotation periods P_{rot}. Data are from *ROSAT* (Table 3; RS fits). *Filled circles*: Hotter PSPC temperature; dashed line represents a power-law regression curve (eq. [1]). *Crosses*: Cooler PSPC temperature. *Open squares*: Ratio between hot and cool EM.

plot in Figures 3*a* and 3*b* the hotter temperature T_{hot} as a function of the *total* L_X using the RS and the MEKAL codes, respectively; obviously, the two parameters are correlated, with

$$L_X \approx 4.3 \times 10^{25} T_{hot}^{4.16\pm0.33} \approx 5.5 \times 10^{25} T_{hot}^{4} [\text{ergs s}^{-1}] \quad (\text{RS}) \tag{5}$$

$$L_X \approx 1.6 \times 10^{25} T_{hot}^{5.09\pm0.34} \approx 1.75 \times 10^{25} T_{hot}^{5} [\text{ergs s}^{-1}] \quad (\text{MEKAL}) \tag{6}$$

(T in MK). Again, $N = 9$, and $R = 0.973$ and $R = 0.978$ for RS and for MEKAL, respectively. Remarkably, this dependence remains valid if we add close binary systems consisting of two almost identical solar-type G stars each: BI Cet (G5 V + G5 V), ER Vul (G1 V + G1 V), and TZ CrB (G0 V + G0 V). We assume that both components of each binary contribute equally to L_X and therefore adopt 50% of the total L_X for one component. The *ROSAT* PSPC results for these binaries are from Dempsey et al. (1993) who used the RS code for their spectral fits; consequently, we display these data on the RS plot (Fig. 3*a*) only, but we wish to emphasize that they have not been used for our linear regression fit. Similar relations have been reported for less restricted star samples (see, e.g., Schrijver et al. 1984; Jordan & Montesinos 1991).

Our stars further fulfill the well-known relation between rotation and L_X, viz.,

$$L_X = 10^{31.05\pm0.12} P_{rot}^{-2.64\pm0.12} [\text{ergs s}^{-1}] \tag{7}$$

($N = 12$, $R = -0.97$; see also Dorren et al. 1995, 1997 and

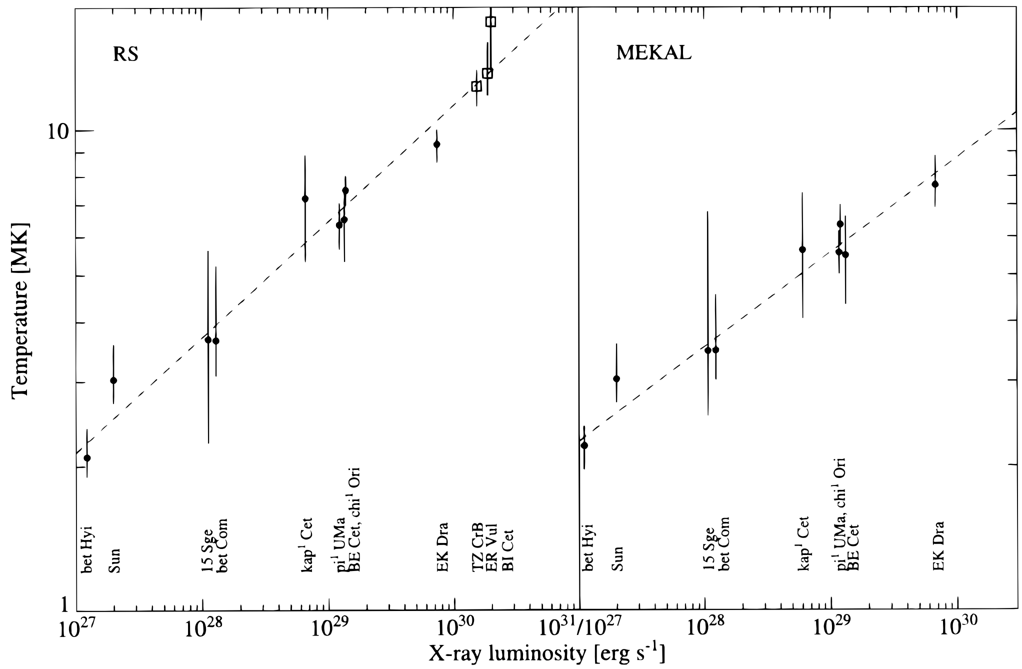

FIG. 3.—Coronal temperature T_{hot} vs. total X-ray luminosity L_X in the [0.1, 2.4] keV energy range from *ROSAT* data, clearly showing a strong correlation. Data are from Table 3. *Left*: From RS fits; *right*: from MEKAL fits. The dashed lines are power-law regression lines, defined by eqs. (5) and (6). The three stars indicated with squares in Fig. 3 (*left*) are close binary systems consisting of two identical G dwarfs each. Data for the binaries are from Dempsey et al. (1993) who used the RS code for their spectral fits.

Maggio et al. 1987 for a larger sample of G stars, and Pallavicini et al. 1981 and Walter 1981 for previous statistics). This fit is plotted in Figure 4 together with the individual data points. The differences between the RS and the MEKAL luminosities are minor. We also plot $\frac{1}{2}L_{X,tot}$ for the three G+G-type RS CVn–like binaries mentioned above; they are obviously much lower than expected from an extrapolation of the regression curve toward smaller rotation periods, indicating "saturation."

The average radio luminosity density L_R (in ergs s^{-1} Hz^{-1}) of active main-sequence stars measured at 5–8.5 GHz appears to be correlated with L_X (Güdel et al. 1995a). Thus, we find (using eq. [5])

$$L_R \approx 1.7 \times 10^{10} T_{hot}^4 [\text{ergs s}^{-1}\ \text{Hz}^{-1}] \tag{8}$$

(T in MK). This seems to imply that microwave-luminous stars are those with hot coronae and that particle acceleration responsible for the observed radio gyrosynchrotron emission is intimately connected with the production of very hot (thermal) plasma (see Güdel 1994 for a review).

4.3. *Results from ASCA*

The results of the 2-T or 3-T fits to the *ASCA* SIS0+1 spectra (SIS0 for HN Peg) are reported in Table 4. In Figure 5, we show the SIS0 spectra with fits of EK Dra, HN Peg, κ^1 Cet, and a simulated nonflare solar spectrum folded with the SIS0 response. For the solar spectrum, we used T and EM as given in Table 3 (adapted from Raymond & Doyle 1981). The spectra have been shifted along the y-axis so as to simulate the count rates if all four stars were at a distance of 10 pc, i.e., close to the distance of κ^1 Cet. Two features are conspicuous: (1) The Fe L-shell peak around 0.8–1 keV shifts to lower energies as L_X decreases, and (2) the slope of the higher energy tail becomes steeper with decreasing L_X. For example, the ratio of the observed X-ray count rate density near 0.8 keV relative to 2 keV is 22, 45, 100, and 1700 for EK Dra, HN Peg, κ^1 Cet, and the Sun, respectively. These features are indicative of the prevalence of *cooler* plasma as the stars become less active.

In view of possible inconsistencies in the spectral codes presently available and the recent findings of elemental "underabundances" in some active stellar coronae (see

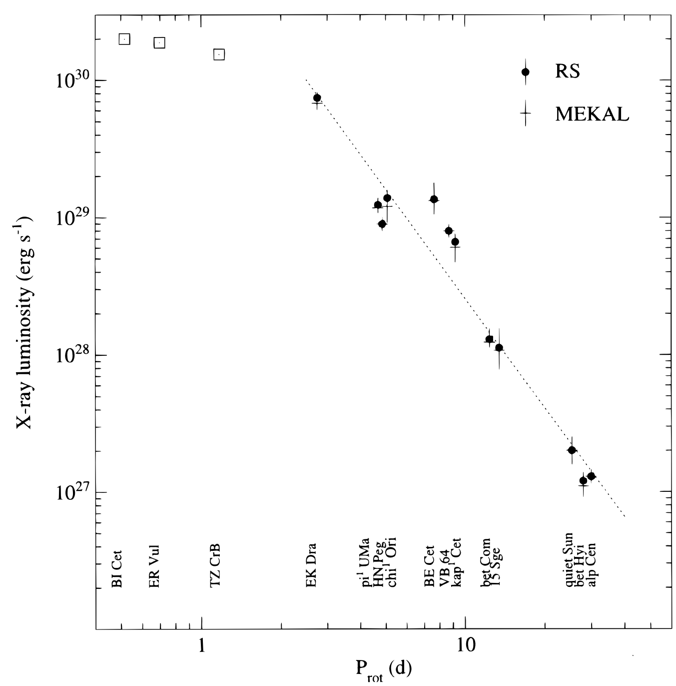

FIG. 4.—X-ray luminosities are plotted as a function of the stellar rotation period. Note the symbols for luminosities derived from RS and from MEKAL fits. The dotted line indicates a linear regression fit (eq. [7]). The three squares give the locations of three RS CVn–like binaries composed of two early-type G V stars each (see text for details). The "saturation" effect for $P_{rot} < 2^d$ is obvious.

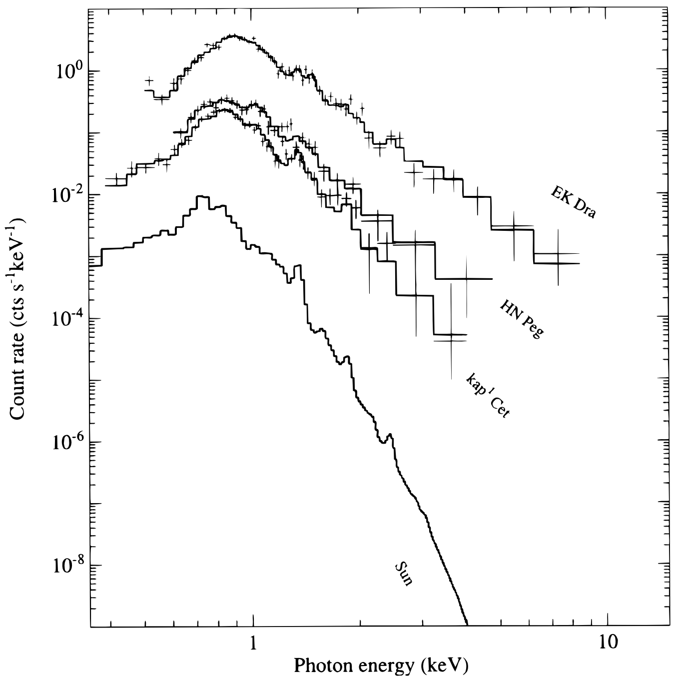

FIG. 5.—Observed *ASCA* SIS0 spectra of (*top to bottom*) EK Dra, HN Peg, κ^1 Cet, and a simulated *ASCA* spectrum for the average nonflaring Sun (model after Table 3). The histograms represent 3-T (2-T in the case of HN Peg) fits to the data (see Table 4). The spectra have been shifted along the *y*-axis so as to represent the three objects at a distance of 10 pc. The steeper high-energy tail and the shift of the spectral peak toward lower photon energies for decreasing X-ray luminosity indicate a decrease in plasma temperature with decreasing activity levels.

White 1996 for a review), it is surprising that both the EK Dra and the κ^1 Cet SIS spectra were well fitted with solar photospheric abundances *except* for Mg, which required a factor of 2.2–2.3 increase relative to solar photospheric despite the two stars' rather different temperature composition (resulting in a considerably different Mg line blend feature for the two stars). In the case of EK Dra, introducing additional fitting parameters like Si and S in combined *ASCA* and *EUVE* spectra lowered the Fe abundance to 83% with only a moderate improvement of the overall fit, and with error margins that were nearly consistent with solar photospheric (Güdel et al. 1997). The HN Peg spectrum was also best fitted with a subsolar Fe abundance, but the deviation is in fact not significant, owing to a rather low S/N (≈ 30 within the energy range considered here). This spectrum shows some residual flux around 1.3 keV that could not be modeled. We note that this feature is most likely artificial and is definitely not due to the Mg abundance since Mg displays its prominent feature at somewhat higher energies. Other elements were either not sufficiently well constrained by the available data or, as in the case of Si, were found to provide the best-fitting result when within 10%–15% of solar photospheric values (an insignificant deviation). We are aware that a good-quality elemental abundance determination requires high S/N spectra and that a number of elements in different blends need to be fitted simultaneously. Our spectra are not adequate to perform this reliably; with two free elemental parameters, we already obtain fits that can barely be improved qualitatively. We therefore adopt only Fe and Mg as free abundance parameters in our *ASCA* fits but mention that high S/N observations with high spectral resolution should be performed in the future, e.g., with the *AXAF* or *XMM* observatories, to resolve the abundance problem for solar-like stars conclusively.

4.4. *DEM Modeling of the ASCA SIS Spectra*

The DEM results are displayed in Figure 6, plotted with similar amplitudes for illustration. All three DEM fits are excellent, with χ^2 values of 126.5 for EK Dra (using 123 spectral bins), 32.7 for HN Peg (33 spectral bins), and 83.9 for κ^1 Cet (88 spectral bins). While the DEM in the temperature range below 2–3 MK is unreliable for HN Peg and κ^1 Cet owing to *ASCA*'s insensitivity to low temperatures, the *ASCA* DEM presented here for EK Dra is very similar to that derived from combined *ASCA* and *EUVE* data; the latter confirms the absence of significant emission measure below ~ 3 MK (Güdel et al. 1997). The DEMs above ~ 3 MK, on the other hand, clearly display evolutionary systematics. In particular, we note the following:

1. The DEM is bimodal in the more active stars, with a minimum emission measure around 10 MK.
2. The total EM of the hotter part decreases rapidly with age; while its amount is comparable to the cooler EM in EK Dra, it diminishes to $\sim 25\%$ at the age of HN Peg

TABLE 4

ASCA 3-T SPECTRAL FIT PARAMETERS: COMPARISON WITH NONFLARING SUN[a]

Parameter	EK Dra	HN Peg	κ^1 Cet	Sun
T_1 [MK]	$6.05^{+1.00}_{-1.29}$	$5.14^{+0.99}_{-3.13}$	$0.98^{+1.1}_{-\cdots}$	1.3[b]
T_2 [MK]	$9.30^{+\cdots}_{-\cdots}$	...	$4.79^{+4.6}_{-0.62}$	3.0[b]
T_3 [MK]	$22.1^{+5.4}_{-3.1}$	$14.55^{+\cdots}_{-3.44}$	$8.11^{+1.3}_{-1.4}$	...
log EM_1 [cm^{-3}]	$51.88^{+0.12}_{-0.29}$	$51.30^{+\cdots}_{-0.24}$	$51.12^{+\cdots}_{-1.0}$	49.63[b]
log EM_2 [cm^{-3}]	$51.80^{+\cdots}_{-0.36}$	...	$50.85^{+\cdots}_{-0.19}$	49.50[b]
log EM_3 [cm^{-3}]	$52.01^{+0.06}_{-0.15}$	$50.83^{+0.18}_{-0.61}$	$50.43^{+0.31}_{-0.29}$	...
$Mg/Mg_{\odot,\mathrm{phot}}$	$2.24^{+0.80}_{-0.55}$	$1.48^{+2.13}_{-0.88}$	$2.30^{+1.1}_{-0.70}$	4.4[c]
$Fe/Fe_{\odot,\mathrm{phot}}$	$0.99^{+0.30}_{-0.20}$	$0.72^{+0.40}_{-0.35}$	$0.98^{+0.37}_{-0.23}$	4.4[c]
log $L_{X,[0.5-10]\,\mathrm{keV}}$ [ergs s^{-1}]	29.70	28.71	28.40	~26.8
log $L_{X,[0.1-2.4]\,\mathrm{keV}}$ [ergs s^{-1}]......	29.77	28.81	28.79	~27.3
χ^2/dof...............................	110/96	24.8/25	74/71	...

[a] All stellar data were fitted with XSPEC Vers. 9.01, using the MEKAL code with variable Fe and Mg on the combined SIS0 + 1 data set (only SIS0 for HN Peg).

[b] Adapted from Raymond & Doyle 1981.

[c] See Drake et al. 1994.

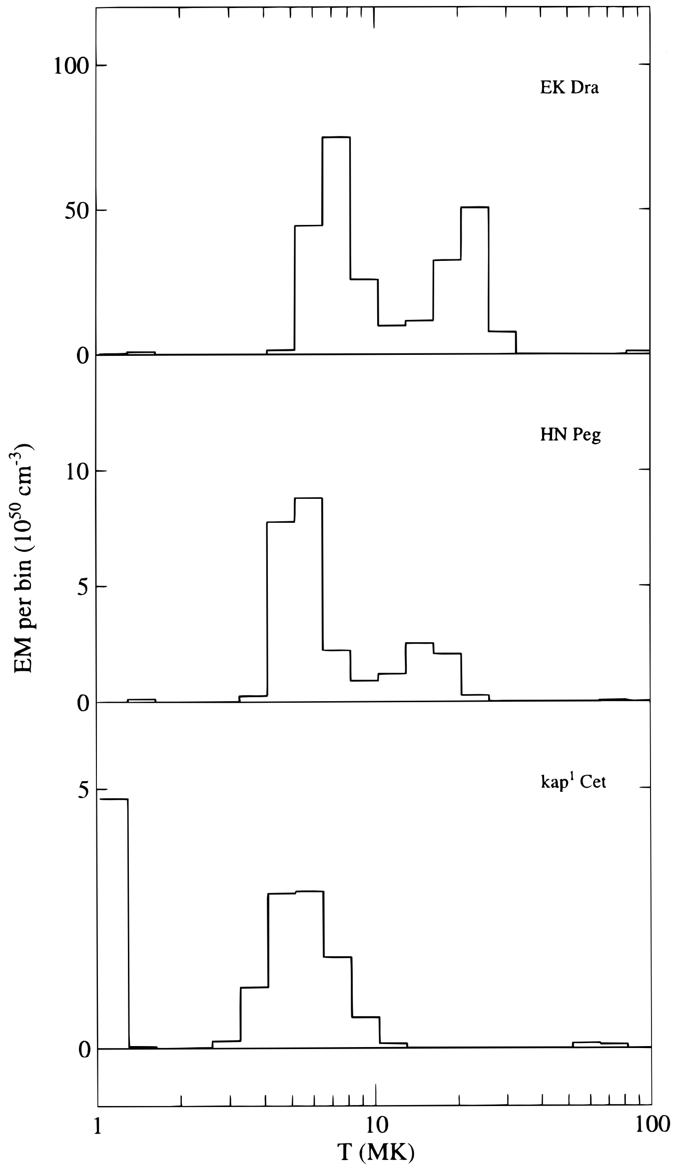

FIG. 6.—Coronal differential emission measure distribution for EK Dra (*top*), HN Peg (*middle*), and κ^1 Cet (*bottom*), derived from *ASCA* SIS data. The DEM distribution becomes unreliable below 3–4 MK owing to the insensitivity of the SIS detectors to such plasmas. For EK Dra, however, the DEM is similar to the *ASCA* and *EUVE* result previously reported by Güdel et al. (1997). A decrease of the high-temperature plasma and a shift of the plasma distribution toward cooler temperatures with increasing age is clearly visible. Note the different EM scales.

($\sim$300 Myr) and becomes undetectable in older stars like κ^1 Cet ($\sim$750 Myr; the small bins just below 100 MK are insignificant residuals).

3. The whole DEM appears to shift slightly toward cooler temperatures with age, with the peak of the hotter plasma at $\sim$(23 $\pm$ 3) MK in EK Dra but at $\sim$(15 $\pm$ 2) MK in HN Peg. The young EK Dra does not show a significant amount of plasma around 3 MK, whereas κ^1 Cet ($\sim$750 Myr) indicates the presence of a considerable EM at such temperatures, although it is not clearly resolvable with *ASCA* (and is probably even underestimated due to the sensitivity limit of the *ASCA* detectors).

For comparison, we mention the DEM analysis of χ^1 Ori by Schrijver et al. (1995) with *EUVE* data. This star is approximately coeval with HN Peg and shows a broad DEM distribution within 2–8 MK; *EUVE* is sensitive to the temperature range below $\sim$10 MK down to 0.1 MK and is therefore ideal to detect the cool coronal plasma (T = 1–3 MK) that we may miss with *ASCA*. Schrijver et al. note a shoulder in the DEM extending from 8 MK out to 15 MK, although its exact location and extent is difficult to assess with *EUVE* data. We suggest that this DEM shoulder in χ^1 Ori is equivalent to the high-temperature bump detected and resolved here in the *ASCA* DEM of HN Peg.

4.5. *The Hot Plasma Component in ROSAT Data*

The spectral resolution of the *ROSAT* PSPC typically allows for fits of up to five independent parameters (corresponding to 5 degrees of freedom comprised in a PSPC spectrum), and in § 4.2, these were chosen to be two emission measures and their associated temperatures and, if required, an interstellar hydrogen absorption column. Fitting more temperature components typically leads to divergences in the temperature fitting (ill-constrained temperature parameters). Nevertheless, 2-T models may be inappropriate for *ROSAT* observations of complicated EM structuring. Indeed, 2-T fitting of *ROSAT* spectra of EK Dra, χ^1 Ori, and π^1 UMa turns out to be of moderate quality (Table 3), showing systematic deviations around 0.5–0.6 keV and at the high-energy end around 1.5–2.5 keV. The observed spectrum above 1.5 keV exceeds the model fit systematically, in particular in the case of EK Dra, which results in comparatively modest χ^2 values (Dorren et al. 1995; see Fig. 7).

We first tested whether the overabundance of Mg (with its feature around 1.4 keV) found in the *ASCA* data could fill in the discrepancy around 1.5 keV. We found that this is not the case in 2-T fits to *ROSAT* data, although there is a slight improvement of the fit around 1.5 keV and below.

On the other hand, with the additional information from the *ASCA* DEMs, the *ASCA*-derived abundances (Fe, Mg), and 3-T fits, we are now in the situation to fit three isothermal components to the *ROSAT* spectra of the more active stars, with the highest temperature held fixed ("$2\frac{1}{2}$-T fits" henceforth; the fitting of the highest S/N observation of EK Dra, obtained in 1991, in fact converged to a highest temperature around 25 MK automatically without any constraints imposed on the fitting procedure). We also fitted the hydrogen absorption columns N_H to keep consistent with the other *ROSAT* spectral fits in view of small calibration uncertainties in the lowest PSPC channels. As a check, we required that it converged close to the value found in the corresponding 2-T fit. Our $2\frac{1}{2}$-T fit results are reported in Table 5, now including two previous pointed PSPC observations of EK Dra (Dorren et al. 1995). The enriched Mg option leads to somewhat better fits, but the high-temperature component is in either case indispensable for filling in the discrepant count rates around 2 keV.

The *ROSAT* $2\frac{1}{2}$-T fit results clearly indicate the presence of very hot plasma in the younger stars, with a fit χ^2 that has considerably improved relative to 2-T fits (e.g., from χ^2 = 214 to χ^2 = 142 for 130 bins in the 1991 observation of EK Dra); the systematic discrepancies between data and fit have almost completely disappeared (Fig. 7). The hot EM has been introduced mainly at the cost of the cool plasma, and this puts the *ROSAT* results into closer agreement with *ASCA*. Note that the crucial intermediate temperatures of the $2\frac{1}{2}$-T fits closely correspond to the high temperature of the 2-T fits and that its emission measure is hardly affected by the redistribution between cool and very hot plasma. We take this as evidence for the physical reality of this com-

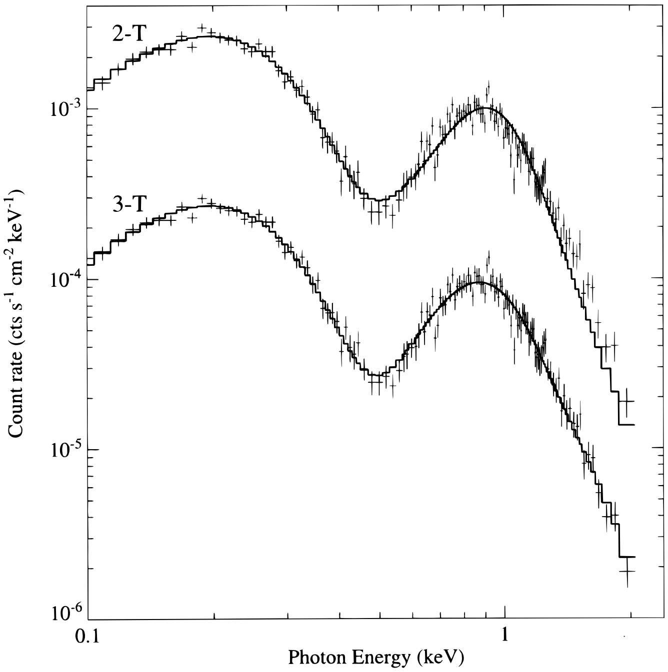

FIG. 7.—*ROSAT* PSPC data of EK Dra, observed in 1991 May (Table 5). Two identical spectra are shown, the lower being shifted by -1 dex along the flux axis for illustration. The fit to the upper version assumes two isothermal plasma components and a variable hydrogen absorption column density. The lower fit additionally includes a third, very hot plasma component with fixed temperature (22 MK) as suggested from the *ASCA* results. Note the discrepancies between data and 2-T fit around 1 keV and the systematically higher data above 1.5 keV.

ponent. The relative amount of hot EM is comparable with the *ASCA* results, although we find a trend for too little hot plasma and too much cold coronal EM. Given the poor spectral resolution of *ROSAT* and the low sensitivity of *ASCA* to $T < 3$ MK, we believe that this result is compatible with the *ASCA* findings.

5. DISCUSSION

5.1. *Coronal Structuring*

We found a consistent trend in the evolution of the hotter plasma: as a solar-like star ages and spins down, the hotter plasma becomes less important. Simple *ROSAT* 2-T fits suggest a decrease of the hotter temperature, while *ASCA* DEM modeling shows that there is also a decrease of the relative amount of emission measure at hotter temperatures. The reliability of temperature determinations with the *ROSAT* PSPC has been simulated and discussed by Maggio et al. (1995). In particular, they find that the presence of two components can be correctly inferred from 2-T fits if the temperatures are well separated and if the ratio of emission measures is greater than 0.5. Temperatures around 15–30 MK can usually be restored only with lower limits since the *ROSAT* PSPC has poor discrimination capabilities for temperatures significantly above 10 MK. Both instrumental restrictions are critical to our stars, which, in the *ASCA* DEMs, show either a considerable amount very hot plasma (EK Dra) or a large ratio between the hot and the cool emission measures. It therefore appears likely that the *ROSAT* results are biased by the increasing weight of the hot plasma in more active stars and that we are not observing a pure temperature effect but a weighted high-temperature average. The *ASCA* DEM results are more likely to yield a correct representation of the true underlying DEM, since individual features and the continuum detected in the *ASCA* spectra are sensitive between ~ 2 MK and several tens of MK.

Before drawing conclusions from our results, we have to discuss the possible systematic effects due to slow, long-term variability, in particular effects on the stellar X-ray luminosity by stellar activity cycles. Several previous studies have systematically compared luminosities of active stars observed with *ROSAT*, *EXOSAT*, and *Einstein*, thus covering a time span of more than one decade (see, e.g., Pallavicini, Tagliaferri, & Stella 1990; Gagné et al. 1995; Schmitt et al. 1995; Micela, Pye, & Sciortino 1997). In general, a scatter of the order of 0.3 dex is found for lower luminosity ($\sim 10^{27}$–10^{28} ergs s^{-1}) stars in the *ROSAT* X-ray band. At higher luminosities, the scatter becomes significantly smaller, apart from possible contamination by frequent flares. By comparing our results with those of Ayres et al. (1995) and Schmitt (1997), we similarly find typical deviations around 0.1 dex or less for these stars for observations that were obtained with the same detector, but years apart. We are therefore mostly concerned with our lower luminosity stars such as β Hyi. For this object, long-term X-ray variability within a factor of 3 has been observed (Dorren et al. 1995). Consulting our Figure 4, we see little evidence for a strong influence of slow variability

TABLE 5

ROSAT $2\frac{1}{2}$-T SPECTRAL FIT PARAMETERS (MEKAL)[a]

Parameter	EK Dra 1991 May 9	EK Dra 1993 Apr 15	EK Dra 1993 Oct 19	π^1 UMa 1993 Oct 5	χ^1 Ori 1992 May 4
Mg abundance	1.0/2.24	1.0/2.24	1.0/2.24	1.0	1.0
Fe abundance..........	1.0/0.99	1.0/0.99	1.0/0.99	1.0	1.0
T_1 [MK]	$1.09^{+0.24}_{-0.41}/1.22^{+0.26}_{-0.33}$	$1.76^{+0.43}_{-0.58}/1.91^{+0.39}_{-0.48}$	$1.67^{+0.57}_{-0.87}/1.90^{+0.48}_{-0.83}$	$1.12^{+0.24}_{-0.19}$	$1.04^{+0.36}_{-0.62}$
T_2 [MK]	$7.04^{+0.42}_{-0.46}/7.17^{+0.43}_{-0.43}$	$6.48^{+0.97}_{-1.0}/6.81^{+0.98}_{-0.99}$	$5.45^{+1.32}_{-1.07}/5.99^{+1.22}_{-1.43}$	$5.05^{+0.95}_{-0.73}$	$5.46^{+0.96}_{-0.94}$
T_3 [MK]	22 fixed	22 fixed	22 fixed	15 fixed	15 fixed
log EM_1 [cm^{-3}]	$52.00^{+0.84}_{-0.12}/51.90^{+0.93}_{-0.09}$	$51.74^{+0.13}_{-0.15}/51.76^{+0.14}_{-0.16}$	$51.60^{+0.25}_{-0.27}/51.69^{+0.22}_{-0.41}$	$51.12^{+0.06}_{-0.07}$	$51.25^{+0.13}_{-0.09}$
log EM_2 [cm^{-3}]	$52.28^{+0.03}_{-0.03}/52.31^{+0.03}_{-0.03}$	$52.14^{+0.03}_{-0.05}/52.16^{+0.04}_{-0.05}$	$52.15^{+0.06}_{-0.08}/52.15^{+0.07}_{-0.07}$	$51.45^{+0.05}_{-0.04}$	$51.36^{+0.04}_{-0.05}$
log EM_3 [cm^{-3}]	$52.38^{+0.07}_{-0.08}/52.23^{+0.10}_{-0.13}$	$52.00^{+0.13}_{-0.21}/51.74^{+0.23}_{-0.58}$	$52.01^{+0.14}_{-0.21}/51.76^{+0.27}_{-0.58}$	$50.67^{+0.34}_{-\cdots}$	$50.66^{+0.26}_{-0.89}$
log $L_{X,[0.5-10]\,keV}$	29.93/29.91	29.73/29.72	29.72/29.70	28.89	28.82
log $L_{X,[0.1-2.4]\,keV}$	30.06/30.04	29.86/29.85	29.83/29.83	29.08	29.06
χ^2/dof..................	(142.4/124)/(137.5/124)	(101.5/92)/(101.1/92)	(79.5/85)/(79.9/85)	86.0/70	65.6/55

[a] All data were fitted with XSPEC Vers. 9.01, using the MEKAL code; for EK Dra, the first numbers refer to solar photospheric abundances, and the second numbers to abundances of 2.24 for Mg and 0.99 for Fe. Errors are 90% confidence limits; if not given, error search did not converge.

on our principal results that cover a range of three orders of magnitude.

We now first discuss possible conclusions from our results based on the model of hydrostatic loops as has frequently been proposed. For a simple hydrostatic loop model with constant cross section and constant heating that is balanced by radiative cooling losses, one finds the two scaling laws (Rosner, Tucker, & Vaiana 1978)

$$T_{\max} = 1.4 \times 10^3 p^{1/3} l^{1/3} [\mathrm{K}] \tag{9}$$

$$\epsilon = 9.8 \times 10^4 p^{7/6} l^{-5/6} [\mathrm{ergs\ s^{-3}}] , \tag{10}$$

where $T_{\max}$ is the maximum temperature, commonly attained at the loop top but being representative for most of the emission measure; the EM distribution reaches significantly cooler temperatures only near the footpoints of the loops. Further, $p = 2nkT$ is the thermal pressure, with n being the electron density and k being the Boltzmann constant; ϵ is the heating rate per unit volume, and l is the semilength of the loop. Equating $L_X = \epsilon V$ (V being the emitting volume), introducing the surface filling factor f for magnetic footpoint areas, and assuming constant cross sections of the loops as a function of height, one derives

$$l = 6 \times 10^{16} T^{7/2} L_X^{-1} f [\mathrm{cm}] \tag{11}$$

(see also Giampapa et al. 1996; we adopt here one solar radius $R_\odot = 7 \times 10^{10}$ cm for the stellar radii). We note that these simple scaling laws are valid for loop heights less than one pressure scale height $\Lambda_p = 5 \times 10^3 T \approx 1.1 \times 10^{11}$ cm, but they can be generalized to heights up to about $2\Lambda_p$ (Serio et al. 1981). Using $L_X \approx 1.8 \times 10^{29}$ ergs s^{-1} (in the [0.1, 10] keV range) and $T \approx 22$ MK for the hotter component in EK Dra, $l = 4.3 \times 10^{12} f$ cm. Either these loops are enormously large ($l \gg \Lambda_p$) and therefore cannot be described in terms of stable, quasi-static loop models or their filling factor must be very small. Solar soft X-ray loops are typically confined to one pressure scale height or less. Under this assumption, the filling factor must be small, $f_{\rm hot} < 0.8\%$. For more typical heights of 10^{10} cm, $f_{\rm hot} < 0.09\%$. Thus, based on hydrostatic loop models, we would predict that the stellar surface is dotted with small compact hot loops, a result that has equally been found by Giampapa et al. (1996) for M dwarfs. For the cooler component in EK Dra, $T \approx 7$ MK; thus, $\Lambda_p = 3.5 \times 10^{10}$ cm. We adopt $L_X = 4.5 \times 10^{29}$ erg s^{-1} for the cooler emission measure. Then, the filling factor $f_{\rm cool} < 27\%$, compatible with the results from a rotational modulation study (Güdel et al. 1995b). We thus infer a somewhat surprising picture of activity in young solar-like stars: Although the most active examples such as EK Dra are close to the empirical "saturation limit" of the magnetic dynamo, typically reached for equatorial rotational velocities of $\sim$15–25 km s^{-1} (see Stauffer et al. 1994; EK Dra's $v_{\rm eq} \approx 17$ km s^{-1}), the corona does not itself appear to be completely filled with X-ray–emitting plasma. However, this view is correct only if quasi-static loops are assumed. We will propose an alternative scenario for the hotter plasma below.

5.2. *The Possible Role of Flares*

The solar corona produces extremely hot plasmas similar to those seen in the hotter stellar DEM peaks only episodically, during flares. The evolution of the flare plasma generally evolves along the following (simplistic) line: Plasma is impulsively heated to high temperatures ($\sim$10–30 MK). The emission measure evolves more gradually as chromospheric material is lifted into the loops; when it peaks, the temperature is already receding owing to conduction and radiation. Finally, coronal material condenses and falls back to the chromosphere, thereby decreasing the X-ray emission measure (see examples in Svestka 1976; Garcia & Farnik 1992; Benz & Güdel 1994; Ding et al. 1996). The range of solar flare temperatures is commensurate with the high-temperature peak in our stellar DEM distributions. Could it be that we are seeing in the stellar DEMs the combined effect of superimposed but temporally unresolved flares occurring during our observations?

We investigate the "unresolved" time-integrated emission measure of a typical solar flare, illustrated by the example shown in Figure 8. The histories of its flux, its temperature, and its emission measure are displayed. The EM and T histories were derived from a 1-T isothermal modeling with *GOES* two-channel data (see Benz & Güdel 1994). We plot in Figure 9*a* a "dynamical" emission measure distribution of the flaring Sun. The histogram on the left, below 4 MK, is a sketch representing the nonflaring Sun (see, e.g., Raymond & Doyle 1981), scaled such that its luminosity is 2×10^{27} ergs s^{-1} in the [0.1,2.4] keV range, a typical value for the inactive Sun. The histogram on the right (above 6 MK) shows the total emission measure at any one temperature attained during the monotonic heating (*dotted line*) and the monotonic cooling phase (*solid lines*) of the flare shown in Figure 8; the histogram thus describes the *trajectory* of the flare on the T-EM plane, with the flare evolution implying the cooling track running from right to left. The flare-heating phase (increasing T) is usually not very important because it shows considerably smaller emission measures than the cooling phase. Below 6–7 MK, the modeling becomes unreliable mainly because of the strongly reduced sensitivity of the *GOES* detectors, but also because of the rapidly decreasing emission measure in the late phase of the flare and consequent problems with the accurate background definition (see Benz & Güdel 1994).

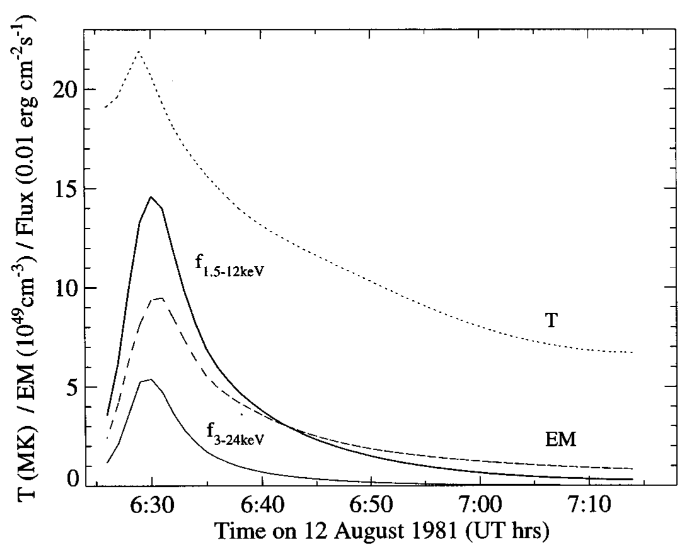

FIG. 8.—Impulsive solar flare on 1981 August 12. The four curves describe the time history of the observed flux in the 1.5–12 keV range as measured by *GOES* (*thick solid line*), the 3–24 keV *GOES* flux (*thin solid line*), the derived temperature (*dotted line*), and the derived emission measure (*dashed line*). The latter two parameters have been computed from the two-channel *GOES* flux data under the assumption of an isothermal plasma. Note the different units on the ordinate.

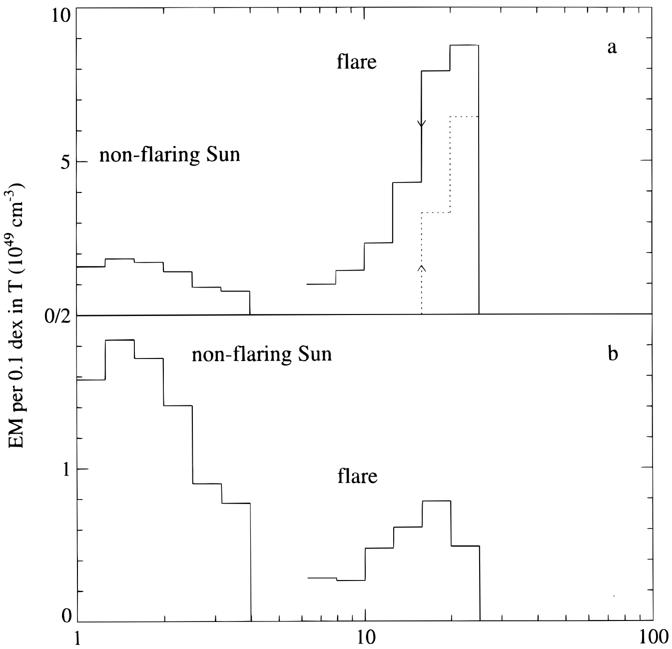

FIG. 9.—Emission measure distribution of the nonflaring Sun (histogram below 4 MK) and the solar flare in Fig. 8 (see text for details on the flare properties). The upper panel (*a*) shows the trajectory of the flare on the T-EM plane, with the "heating" branch of the flare shown dotted and the cooling branch shown by solid lines. In the bottom panel (*b*), the flare EMs have been weighted by the dwell time of the flare within each temperature bin and normalized by the total flare observing time (48 minutes). Note the different scale of the ordinate on the two panels. Compare this EM distribution with the DEMs found from *ASCA* observations of active solar-type stars (Fig. 6).

The "hot," flare component of the emission measure reaches up to 1×10^{50} cm^{-3} at a given time, while the *integrated* cool plasma amounts to approximately 8×10^{49} cm^{-3}. The flare selected here is a rather small impulsive event, with a peak luminosity of approximately 1×10^{27} ergs s^{-1} in the [0.1,2.4] keV band during the cooling phase and a characteristic soft X-ray duration of 29 minutes.

A time-integrated observation will detect the emission measure $\mathrm{EM}(T)'$ in the temperature interval $[T, T + \Delta T]$, where $\mathrm{EM}(T)'$ is the amount of emission measure attained at a temperature T weighted with the dwell time δt of the flare within $[T, T + \Delta T]$ and normalized with the total observing time Δt; thus, $\mathrm{EM}(T)' = \mathrm{EM}(T) \times \delta t/\Delta t$; for the solar flare, we used $\Delta t = 48$ minutes, after which time the flare emission measure has decayed to about 9% of the peak and the temperature has receded to 6–7 MK. The observation will thus recover the apparently static emission measure distribution shown in Figure 9*b* emulated by the trajectory in Figure 9*a*. This distribution is to be compared with the stellar DEMs in Figure 6. The observed amplitude of the integrated emission measure will, for a given number distribution of flare amplitudes, be proportional to the flare frequency. We note in passing that the hydrostatic loop models discussed in § 5.1 are *not* necessarily correct for flaring loops that are presumably heated impulsively and then gradually cool back to an equilibrium owing to radiative and conductive losses. Therefore, the strong constraints for possible surface filling factors for hot plasma do not necessarily apply.

Our tentative interpretation of the decline of *average* coronal temperatures with increasing age is thus a dynamical one: We suggest that the main parameter to determine the hot temperature tail of the coronal DEM is the *flare frequency*. As it diminishes with decreasing activity levels, the relative amount of plasma heated to temperatures above 10 MK in flaring events becomes less important on a time average, and so the overall emission measure distribution declines to lower temperatures. This interpretation may not be unequivocal. However, the evidence accumulated here makes a consideration of a flare-based model for the "quiescent" coronae worthwile. It has the advantage of providing a natural link between the DEM distribution of hot active stars to the "bimodal" structure on the Sun, i.e., cool regions in the nonflaring Sun and hot loops during flares (Figs. 9*a* and 9*b*).

5.3. *The Connection to High-Energy Phenomena*

The high-temperature component of EK Dra is interesting in the context of microwave radiation. Of the sample of G stars that have been discussed here, only EK Dra has been positively detected as a steady, "quiescent" microwave source (Güdel et al. 1994, 1995b). This radiation is interpreted as synchrotron radiation from a population of nonthermal, accelerated electrons. In contrast, π^1 UMa and HN Peg remained undetected in a rather deep VLA[2] integration (Güdel et al. 1995a). RS CVn binary stars also show a high-temperature X-ray component (see, e.g., Dempsey et al. 1993), and they are at the same time efficient radio emitters (Drake, Simon, & Linsky 1989). In solar flares, gyrosynchrotron microwave emission is produced along with high-temperature (20–30 MK) plasma, while the quiescent, "cool" corona does not give rise to measurable gyrosynchrotron radiation. Furthermore, the microwave emission of very active stars is correlated with the X-ray luminosity (which, for these stars, is predominantly determined by the higher temperature plasma), a correlation that applies equally for solar flares (see Güdel & Benz 1993; Benz & Güdel 1994). Taken together, this evidence seems to suggest that the presence of a hot plasma component (and not only a high X-ray luminosity) is conditional for the detectability of a late-type (solar-like) star as a strong, nonthermal radio source (see also Güdel et al. 1995a for a sample of F- and G-type radio stars). Indeed, we infer from equation (8) that the radio luminosity tends to be large in stars with hot coronae, although we understand that an empirical correlation is no proof for a physical relation. Nevertheless, it does provide a second piece of evidence for our hypothesis that the hot coronal plasma is due to flares. In solar flares, the very hot plasma and the nonthermal electron population are *physically* and *causally* related (see, e.g., Hudson & Ryan 1995 for a review). And finally, to close this chain of arguments, Güdel et al. (1996a) found in a study of chromospheric evaporation on an active flare star that the ratio between the flare radiative energies emitted in the soft X-rays and in the radio domain is the same as the luminosity ratio observed for the "quiescent" state. This, then, gives a direct hint for the possible underlying cause both (1) for the relation between "quiescent" X-ray and radio emission and (2) for the association between radio emission and hot coronal plasma, viz., coronal heating by flares.

[2] The VLA is a facility of the National Radio Astronomy Observatory, which is operated by Associated Universities, Inc., under cooperative agreement with the National Science Foundation.

5.4. *Saturation*

The characteristics of saturation in solar-type stars can now be quantified more precisely. Saturation occurs at a level of $L_X/L_{bol} \approx 10^{-3}$ both for single or binary stars (Vilhu 1984; Vilhu & Walter 1987), with which our results agree: From Figure 4, L_X appears to be approximately 2×10^{30} ergs s^{-1}, which is suggested from the location of the G-type close binaries. The break in the power-law relation appears to occur at $P_{rot} = 2$–2.5 days or $v \sin i = 20$–25 km s^{-1} with an X-ray output of $L_X \approx 10^{30}$ ergs s^{-1}. This is in a regime in which about one-third of the emission measure resides at temperatures above 10 MK.

Does saturation occur for radio emission from high-energy electrons? For EK Dra, $L_X/L_R \approx 10^{15.8}$ Hz (Güdel et al. 1995a), a value that is somewhat higher than for very active late-type stars ($\sim 10^{15.5}$ Hz) of which some are close to or slightly within the saturation level (a mid-M dwarf saturates for periods of about 5 days; see Vilhu et al. 1989). The rapidly rotating G stars that are deep into saturation (the three G+G close binaries discussed above) have $L_X/L_R \approx 10^{14.42-14.64}$ Hz (Drake et al. 1989), i.e., they are radio overluminous relative to a nonsaturated star by a factor of 10. Extrapolating equation (7) to their rotation periods would predict $\log L_X = 30.9$–31.8, and thus $L_X/L_R \approx 10^{15.35-15.92}$ Hz, which is compatible with the value found for EK Dra.

We illustrate this effect in Figure 10, where we plot the X-ray luminosity L_X and the radio luminosity L_R (typically at frequencies of 5–8.5 GHz; both luminosities normalized by L_{bol}) for the more active stars in our sample as a function of P_{rot}; we have shifted L_R by 15.5 dex for illustration. The radio data of the G-star binaries are from Drake et al. (1989), and we again adopt 50% of the total luminosity for each of the two identical components. The L_{bol} values are from Drake et al. (1989; BI Cet was corrected to the distance given by Dempsey et al. 1993) or were computed from visual magnitudes and distances (Gliese 1969; Dorren & Guinan 1994a), assuming standard bolometric corrections. We include other stars that fit into our sample and for which radio detections exist, but in order to avoid ambiguities owing to different internal structuring and size, we exclude any non–G-type stars and also avoid pre–main-sequence objects. Thus, two new stars are included in our sample, although both are borderline cases: The little-known HD 181321 = Gl 755 has been detected among the first radio G stars, and its $v \sin i$ allows us to put upper limits only on P_{rot} (Güdel et al. 1994, 1995a). Further, H II 1136 is a Pleiades G8 V star (and therefore somewhat cooler than our G stars) detected in the microwaves by Lim & White (1995); its L_X is from Stauffer et al. (1994).

From Figure 10, we see that as L_X saturates, *the radio emission appears to be little influenced by the effects that saturate the X-rays*, at least for our rather restricted sample of solar-type stars and within the margins that we can consider here, i.e., a factor of 10 in the ratio L_X/L_R. Saturation may well occur beyond this limit, and this is suggested by a considerably weaker dependence of L_R on P_{rot} among the four rapid rotators ($P_{rot} < 1.5$ days). At this point, it must suffice to state that saturation of radio emission is prevented around the onset of the X-ray saturation and that radio emission continues to increase with decreasing rotation (at least) until it reaches an excess luminosity relative to the X-rays by a factor of ~ 10.

The less effective saturation effect in radio emission finds support in other star samples: From the tables and plots in Drake et al. (1989), we find that RS CVn binaries with $P_{rot} > 10$ days mostly show $L_X/L_R > 10^{15.0}$ Hz (typical range: $10^{15.2 \pm 0.4}$ Hz), while the rapid rotators with $P_{rot} <$ 10 days are radio overluminous, i.e., $L_X/L_R < 10^{15.0}$ Hz (typical range: $10^{14.4 \pm 0.5}$ Hz), although we caution that this sample is inhomogeneous, comprising giants, subgiants, and main-sequence stars of various spectral types, with perhaps largely differing saturation levels or even saturation mechanisms. For a further discussion of enhanced radio activity relative to X-ray emission, see Guinan & Giménez (1993).

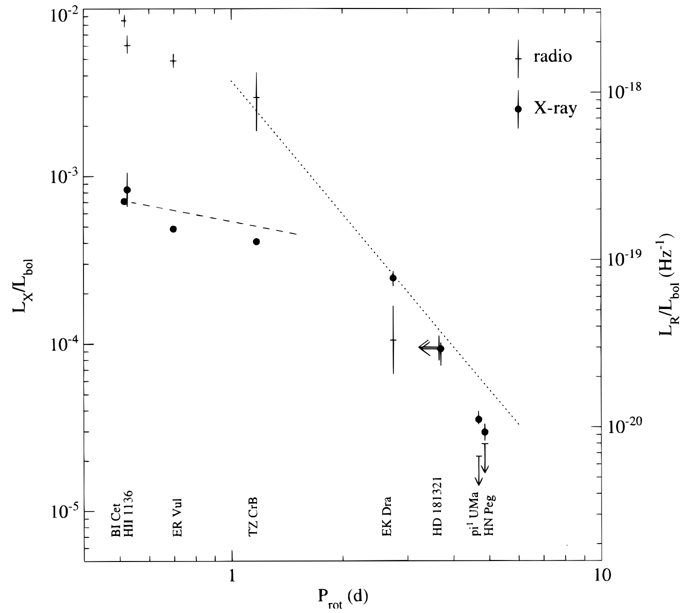

FIG. 10.—Radio (*crosses*) and X-ray (*filled circles*) luminosities of single and binary solar-type G stars plotted as a function of rotation period. Only fast rotators are considered here. The radio axis is shifted against the X-ray axis by 15.5 dex for illustration. Note that saturation occurs for the X-ray emission around $P_{rot} \approx 2^d$, while the radio luminosity continues to increase toward smaller P_{rot}. The dotted line is the fit to the X-ray luminosities from Fig. 4. The dashed line schematically indicates the saturation effect in X-ray emission. See text for details on sources and references.

This result may find a natural explanation in the context of coronal flares. A well-accepted picture of what happens in most solar flares (and presumably in stellar flares) is subsumed in the chromospheric evaporation scenario (see, e.g., Hudson & Ryan 1995 for a review). There is increasing evidence that a large part of the initial flare energy is released in energetic, nonthermal particles that travel from the acceleration region high in the corona along the magnetic field lines toward the loop footpoints. In the lower layers, in particular in the chromosphere, the electrons are braked and transform their energy into heat. The increasing pressure drives heated chromospheric material upward into the low-density coronal loops. This "chromospheric evaporation" fills magnetic loops with hot, dense plasma. Saturation in this picture is consistent with having all available loops at relatively high density and at high, "flarelike" temperatures so that additional energetic particles streaming down from high coronal energy release sites will not increase the X-ray luminosity, although those with large pitch angles will continue to radiate gyrosynchrotron emission.

5.5. *The Dependence of Activity on Age*

Main-sequence stars lose angular momentum via a magnetized wind; their spin-down in turn weakens the magnetic dynamo. Owing to this feedback mechanism, the rotation period has, at an age of ~ 500 Myr, converged to a characteristic value (~ 7 days) that is independent of the initial angular momentum (see Soderblom et al. 1993). From then on, age and rotation rate are uniquely dependent, and the question on whether age or rotation rate is the primary determinant for X-ray activity becomes moot for single stars.

For G stars with ages beyond a few 100 Myr, the X-ray luminosity diminishes in concert with the rotation period. Our narrow sample implies an age dependence law (using the rotation-age relation given in Dorren et al. 1997)

$$L_{\rm X} \approx 2.1 \times 10^{28} t^{-1.5} [\rm ergs\ s^{-1}] \tag{12}$$

(t in Gyr), in excellent agreement with Maggio et al. (1987); their power-law exponent is $-(1.5^{+0.3}_{-0.2})$. Results involving exponential decays have also been reported from other star samples (see Walter & Barry 1991 and Simon 1992 for reviews). Within our sample of nonsaturated stars, a power-law decay describes the observed behavior sufficiently well.

Our study finds a rapid evolutionary decay of the amount of hot material in stellar coronae, on a timescale of approximately 500 Myr in the younger stars. This appears to be the same timescale as that found for the decay of nonthermal radio emission (Güdel 1996). As a consequence, the radiated X-ray emission rapidly becomes softer in energy, with important implications on the ionization of young planets' atmospheres (see, e.g., Ayres 1996).

Finally, we discuss the apparent dichotomy between active dKe and dMe stars that systematically show high-temperature plasma along with a cooler component and F and G main-sequence stars that appear to exhibit, if at all, a much less significant high-temperature component (Schmitt et al. 1990). Apart from the low-resolution fitting problems we encountered in § 4.5, we first of all do find examples with a high-temperature component, but this population is admittedly rather small, with stars beyond the age of the Hyades typically not showing a considerable EM component beyond 10 MK. On the other hand, given that the spin-down time for a G star is about 10 times shorter than for an M dwarf (Soderblom et al. 1993) and the principal parameter determining magnetic activity being the rotation period, the fraction of very active F and G stars must be considerably smaller than the fraction of active dMe stars among all M dwarfs. If the birthrate of G stars were constant, only one out of 20 field G stars in the solar neighborhood could be expected to be sufficiently young to support a "quiescent" hot coronal plasma. An analogous effect with the same decay timescale has been noted for microwave activity (Güdel 1996).

6. THE SOLAR-STELLAR CONNECTION: A SYNOPSIS

The main point of our paper is, by referring to the characteristic DEMs that we have derived and by arguing with the detectable high-energy electrons seen in the radio emission, that flare heating may be the ultimate cause for the high-temperature bump in the observed coronal X-ray emission measure distribution of solar-type stars. While the flare-heating hypothesis is not new and still awaits an unambiguous proof, we have added a number of new pieces to the line of evidence:

1. We find that the hotter plasma constitutes a separate emission measure component characteristically distributed above 10 MK, reaching temperatures up to about 30 MK. The distribution is reminiscent of the time-integrated DEM of solar flares.
2. Our paper finds, and we believe for the first time, how 2-T domains of plasma evolve into a single-peaked cooler EM distribution, i.e., by the reduction of the hot plasma component rather than simple cooling. This is expected from the flare scenario since older, less active stars produce strongly heating flares less frequently.
3. The DEM distribution with its minimum around 10 MK is reminiscent of the inverse of the plasma cooling function, which sharply decreases from 10 to 15 MK, thus suggesting that we are observing cooling loops.
4. The flare scenario, involving chromospheric evaporation, is consistent with the observation that in very active, "saturated" stars there is little or no cool plasma (of a few MK) because it is rapidly reprocessed by heating events. The relative amount of very hot EM increases with increasing activity.
5. From a statistical point of view, the radio-luminous stars are those that support large amounts of *hot* emission measure.

Investigating a sequence of stars that are analogs of the Sun at different ages, we have obtained results on the coronal temperature structuring that are potentially important for an understanding of our own Sun's past. The physical properties of its ionizing radiation (e.g., its hardness and spectral structure) are of prime relevance for the evolution of the young planetary atmospheres (see, e.g., Ayres 1996). Taken together with our previous investigations on the "Sun in Time," the present study allows us to draw a speculative although verifiable sketch of the long-term evolution of the solar corona. As the Sun settles onto the main sequence, the internal magnetic dynamo generates considerable magnetic surface activity with a large volume filling factor of magnetic loops. Frequent flare events are initiated by reconnection of magnetic fields. These release a considerable fraction of their initial energy in fast particles, heating loop systems to 20–30 MK, with repetitive events favoring heating to extreme temperatures. The densities in flare loops are rather high, so that a large fraction of the observed emission measure resides in cooling postflare loops. This emission is observed as the time-integrated high-temperature bump in the DEM reconstructions of very active stars.

In the most rapidly rotating stars, the X-ray corona is "saturated," while radio emission does not appear to go into a similarly strict saturation regime. We can only speculate that perhaps the increasing conductive losses near the loop footpoints of hot loops may balance larger increases in X-ray emission measure while such a constraint does not exist for the acceleration mechanism of particles. Full X-ray saturation would be equivalent to having all available loops filled with dense hot flare plasma. A saturated star will reveal little or no evidence of cool coronal plasma, since the latter is reprocessed quickly and is reheated to flare temperatures by fast electrons. While observational support for this picture is needed, its consistency provides evidence that the *primary* energy release in solar-type coronae occurs via acceleration of charged particles to high energies (>10 keV for electrons).

As the Sun gets older, its magnetic activity and the magnetic surface filling factor decline, implying less frequent flaring events until, after perhaps 500 Myr, hot coronal flares become isolated events in time. Beyond that time, flares transiently heat parts of the corona to >10 MK and release nonthermal particles only episodically.

We are grateful for constructive comments by Benjamin Montesinos, who reviewed our paper, and a second, anonymous referee. We thank the staff at ISAS and GSFC for their invaluable help during scheduling of *ASCA* observations and processing of *ASCA* data; in particular, we acknowledge support by Keith Arnaud during the initial *ASCA* data analysis, and helpful discussions with Koji Mukai during our data processing. We profited from help by Howard Garcia (NIST, Boulder) and Eric Kihn (NOAA, Boulder) in the analysis of *GOES* X-ray data. M. G. acknowledges the hospitality of the Astronomy Department at Villanova University, JILA/University of Colorado, SRON in Utrecht, and the Institute of Astronomy/ETH Zürich during his visits. He thanks the Utrecht group (in particular, Rolf Mewe and Jelle Kaastra) for their help during installation of and familiarizing with the SPEX software package. E. F. G. acknowledges support from PSI during his visit. S. S. acknowledges support from the Japan Society for the Promotion of Science and NASA grant NAGW-4673. This work was supported by NASA grants NAG 5-2494 for *ROSAT* and NAG 5-2707 for *ASCA* to Villanova University.

REFERENCES

Ayres, T. R. 1996, J. Geophys. Res. Planets, in press
Ayres, T. R., et al. 1995, ApJS, 96, 223
Barbera, M., Micela, G., Sciortino, S., Harnden, F. R., Jr., & Rosner, R. 1993, ApJ, 414, 846
Benz, A. O., & Güdel, M. 1994, A&A, 285, 621
Brickhouse, N. S. 1996, in IAU Colloq. 152, Astrophysics in the Extreme Ultraviolet, ed. S. Boywer & R. F. Malina (Dordrecht: Kluwer), 105
Bruner, M. E., & McWhirther, R. W. P. 1988, ApJ, 326, 1002
Caillault, J.-P., & Helfand, D. J. 1985, ApJ, 289, 279
Dempsey, R. C., Linsky, J. L., Schmitt, J. H. M. M., & Fleming, T. A. 1993, ApJ, 413, 333
Ding, M. D., Watanabe, T., Shibata, K., Sakurai, T., Kosugi, T., & Fang, C. 1996, ApJ, 458, 391
Dorren, J. D., Güdel, M., & Guinan, E. F. 1995, ApJ, 448, 431
Dorren, J. D., & Guinan, E. F. 1994a, in IAU Colloq. 143, The Sun as a Variable Star, ed. J. M. Pap et al. (Cambridge: Cambridge Univ. Press), 206
———. 1994b, ApJ, 428, 805
Dorren, J. D., Guinan, E. F., & DeWarf, L. E. 1997, submitted
Drake, S. A. 1996, in ASP Conf. Proc. 99, Cosmic Abundances: 6th Annual Astrophysics Conference in Maryland, ed. S. S. Holt & G. Sonneborn (San Francisco: ASP), in press
Drake, J. J., Laming, J. M., & Widing, K. G. 1995, ApJ, 443, 393
Drake, S. A., Simon, T., & Linsky, J. L. 1989, ApJS, 71, 905
Drake, S. A., Singh, K. P., White, N. E., & Simon, T. 1994, ApJ, 436, L87
Dravins, D., Linde, P., Ayres, T. R., Linsky, J. L., Monsignori-Fossi, B., Simon, T., & Wallinder, F. 1993a, ApJ, 403, 412
Dravins, D., Linde, P., Fredga, K., & Gahm, G. F. 1993b, ApJ, 403, 396
Dravins, D., Lindgren, L., Nordlund, A., & VandenBerg, D. A. 1993c, ApJ, 403, 385
Dupree, A. K., Brickhouse, N. S., Doschek, G. A., Green, J. C., & Raymond, J. C. 1993, ApJ, 418, L41
Dupree, A. K., Brickhouse, N. S., & Hanson, G. J. 1996, in IAU Colloq. 152, Astrophysics in the Extreme Ultraviolet, ed. S. Boywer and R. F. Malina (Dordrecht: Kluwer), 141
Gagné, M., Caillault, J.-P., & Stauffer, J. R. 1995, ApJ, 450, 217
Garcia, H. A., & Farnik, F. 1992, Sol. Phys., 141, 127
Giampapa, M. S., Rosner, R., Kashyap, V., Fleming, T. A., Schmitt, J. H. M. M., & Bookbinder, J. A. 1996, ApJ, 463, 707
Gliese, W. 1969, Catalogue of Nearby Stars. Veröffentl. des Astron. Recheninstituts Heidelberg, No. 22
Güdel, M. 1994, ApJS, 90, 743
———. 1996, in ASP Conf. Proc. 93, Radio Emission from the Stars and the Sun, ed. A. R. Taylor & J. M. Paredes (San Francisco: ASP), 285
Güdel, M., & Benz, A. O. 1993, ApJ, 405, L63
Güdel, M., Benz, A. O., Schmitt, J. H. M. M., & Skinner, S. L. 1996a, ApJ, 471, 1002
Güdel, M., & Guinan, E. F. 1996, in Astrophysics in the Extreme Ultraviolet, ed. S. Bowyer and R. F. Malina (Dordrecht: Kluwer), 519
Güdel, M., Guinan, E. F., Mewe, R., Kaastra, J. S., & Skinner, S. L. 1997, ApJ, 479, 416
Güdel, M., Guinan, E. F., & Skinner, S. L. 1996b, in Röntgenstrahlung from the Universe, ed. U. Zimmermann, J. E. Trümper, & H. Yorke (MPE Special Report 263) (Garching: MPE), 39
Güdel, M., Schmitt, J. H. M. M., & Benz, A. O. 1994, Science, 265, 933
———. 1995a, A&A, 302, 775
Güdel, M., Schmitt, J. H. M. M., Benz, A. O., & Elias, N. M., II. 1995b, A&A, 301, 201
Guinan, E. F., et al. 1997, in preparation
Guinan, E. F., & Giménez, A. 1993, in The Realm of Interacting Binary Stars, ed. J. Sahade et al. (Dordrecht: Kluwer), 51
Hempelmann, A., Schmitt, J. H. M. M., Schultz, M., Rüdiger, G., & Stępień, K. 1995, A&A, 294, 515
Hudson, H., & Ryan, J. 1995, AR&A, 33, 239
Jordan, C., & Montesinos, B. 1991, MNRAS, 252, 21P
Kaastra, J. S., Mewe, R., Liedahl, D. A., Singh, K. P., White, N. E., & Drake, S. A. 1996a, A&A, 314, 547
Kaastra, J. S., Mewe, R., & Nieuwenhuijzen H. 1996b, in UV and X-Ray Spectroscopy of Astrophysical and Laboratory Plasmas, ed. K. Yamashita & T. Watanabe (Tokyo: Universal Academy), 411
Landini, M., Monsignori Fossi, B. C., Pallavicini, R., & Piro, L. 1986, A&A, 157, 217
Lemen, J. R., Mewe, R., Schrijver, C. J., & Fludra, A. 1989, ApJ, 341, 474
Lim, J., & White, S. M. 1995, ApJ, 453, 207
Maggio, A., et al. 1987, ApJ, 315, 687
Maggio, A., Sciortino, S., Collura, A., & Harnden, F. R., Jr. 1995, A&AS, 110, 573
Mewe, R., Gronenschild, E. H. B. M., & van den Oord, G. H. J. 1985, A&AS, 62, 197
Mewe, R., Kaastra, J. S., & Liedahl, D. A. 1995, Legacy, 6, 16
Mewe, R., Kaastra, J. S., van den Oord, G. H. J., Vink, J., & Tawara, Y. 1997, A&A, in press
Mewe, R., Kaastra, J. S., White, S. M., & Pallavicini, R. 1996, A&A, 315, 170
Micela, G., et al. 1985, ApJ, 292, 172
Micela, G., Pye, J., & Sciortino, S. 1997, A&A, in press
Pallavicini, R., Golub, L., Rosner, R., Vaiana, G. S., Ayres, T., & Linsky, J. L. 1981, ApJ, 248, 279
Pallavicini, R., Tagliaferri, G., & Stella, L. 1990, A&A, 228, 403
Pfeffermann, E., et al. 1986, Proc. SPIE, 733, 519
Raymond, J. C. 1988, in Hot Thin Plasmas in Astrophysics, ed. R. Pallavicini (Dordrecht: Kluwer), 3
Raymond, J. C., & Doyle, J. G. 1981, ApJ, 245, 1141
Raymond, J. C., & Smith, B. W. 1977, ApJS, 35, 419
Rosner, R., Tucker, W., & Vaiana, G. S. 1978, ApJ, 220, 643
Rucinski, S. M., Mewe, R., Kaastra, J. S., Vilhu, O., & White, S. M. 1995, ApJ, 449, 900
Schmitt, J. H. M. M. 1997, A&A, 318, 215
Schmitt, J. H. M. M., Collura, A., Sciortino, S., Vaiana, G. S., Harnden, F. R., Jr., & Rosner, R. 1990, ApJ, 365, 704
Schmitt, J. H. M. M., Fleming, T. A., & Giampapa, M. S. 1995, ApJ, 450, 392
Schmitt, J. H. M. M., Golub, L., Harnden, F. R., Jr., Maxson, C. W., Rosner, R., & Vaiana, G. S. 1985, ApJ, 290, 307
Schrijver, C. J., Mewe, R., & Walter, F. M. 1984, A&A, 138, 258
Schrijver, C. J., van den Oord, G. H. J., Mewe, R., & Kaastra, J. S. 1995, A&A, 302, 438
Serio, S., Peres, G., Vaiana, G. S., Golub, L., & Rosner, R. 1981, ApJ, 243, 288
Simon, T. 1992, in ASP Conf. Proc. 26, 7th Workshop on Cool Stars, Stellar Systems, and the Sun, ed. M. S. Giampapa & J. A. Bookbinder (San Francisco: ASP), 3
Simon, T., Herbig, S., & Boesgaard, A. M. 1985, ApJ, 293, 551
Simon, T., & Landsman, W. 1991, ApJ, 380, 200
Skumanich, A. 1972, ApJ, 171, 565
Soderblom, D. R., Stauffer, J. R., Hudson, J. D., & Jones, B. F. 1993, ApJS, 85, 315
Sonett, C. P., Giampapa, M. S., & Matthews, M. S., ed. 1991, The Sun in Time (Tucson: Univ. of Arizona Press)
Stauffer, J. R., Caillault, J.-P., Gagné, M., Prosser, C. F., & Hartmann, L. W. 1994, ApJS, 91, 625
Svestka, Z. 1976, Solar Flares (Dordrecht: Kluwer)
Tanaka, Y., Inoue, H., & Holt, S. S. 1994, PASJ, 46, L37
Vilhu, O. 1984, A&A, 133, 117
Vilhu, O., Ambruster, C. W., Neff, J. E., Linsky, J. L., Brandenburg, A., Ilyin, I. V., & Shakovskaya, N. I. 1989, A&A, 222, 179
Vilhu, O., & Walter, F. M. 1987, ApJ, 321, 958
Walter, F. M. 1981, ApJ, 245, 677
Walter, F. M., & Barry, D. C. 1991, in The Sun in Time. ed. C. P. Sonett, M. S. Giampapa, & M. S. Matthews (Tucson: Univ. of Arizona Press), 633
White, N. E. 1996, in ASP Conf. Proc. 109, Cool Stars, Stellar Systems, and the Sun, ed. R. Pallavicini & A. K. Dupree (Proc. 9th Cambridge Workshop) (San Francisco: ASP), 193